Joint International Topical Meeting on Mathematics & Computation and Supercomputing in Nuclear Applications (M&C + SNA 2007)
Monterey, California, April 15-19, 2007, on CD-ROM, American Nuclear Society, LaGrange Park, IL (2007)

RADIATION INTERACTION ANALYSIS FOR BWR CHANNEL SHADOW CORROSION

Ren-Tai Chiang
University of Florida
231 Nuclear Science Building, Gainesville, FL 32611, USA
rchiang@UFL.edu

Aylin Yilmazbayhan
Electric Power Research Institute
3420 Hillview Ave., Palo Alto, CA 94304, USA
ayilmazb@epri.com

ABSTRACT

Radiation fields (neutron-gamma-electron) across the fuel channel, water gap, and control blade in a control cell of an operating BWR with and without control blade insertion are computed using MCNP5 to shed a light on understanding of the radiation effect on the BWR fuel channel shadow corrosion. MCNP modeling results show that there is practically no flux difference for neutron above 100 eV and for photon above 100 keV due to long neutron and gamma mean free paths but the low energy electron fluxes show some differences among fuel channel, water and control blade. The low energy electron flux differences are primarily due to three factors: 1) short range of electrons, 2) dependence of Compton- and photon-electron productions on different atomic number Z among channel, water and control blade, and 3) dominance of photoelectron production (approximately proportional to Z^4/E^3) from low energy photons in high Z material. A net electron flow from the fuel channel to the control blade is possible only if a severe channel bow occurs such that the distance between the channel and the blade is less than 0.089 cm. This may enhance the channel shadow corrosion.

Key Words: Effect of Radiation, Shadow Corrosion, Channel Bow, BWRs

1. INTRODUCTION

In the recent years, accelerated corrosions on BWR fuel channels next to control blade and on BWR fuel cladding next to inconel spacer grids have been serious problems in the nuclear industry. The accelerated corrosions are in the form of a shadow of non-zirconium alloy component in proximity, and hence the term "shadow corrosion" is used.

Exposure of the fuel channels to the stainless steel control blade can lead to shadow corrosion on the channel surface, resulting in enhanced corrosion induced hydrogen pickup and leading ultimately to greater dimensional change on the side facing to the control blade. In extreme cases, channel bow due to shadow corrosion on the channel surface and fast neutron fluence gradient across the channel has resulted in inoperable control blades by closing the gap between fuel channel and control blade. Especially in C- and S-lattice BWRs, severe shadow corrosion

induced channel bow was observed because of the smaller water gaps between fuel channel and control blade. A typical shadow corrosion formed on the fuel channel surface next to the control blade can be seen in Figure 1 in which the control blade handle shows up on the fuel channel quite clearly.

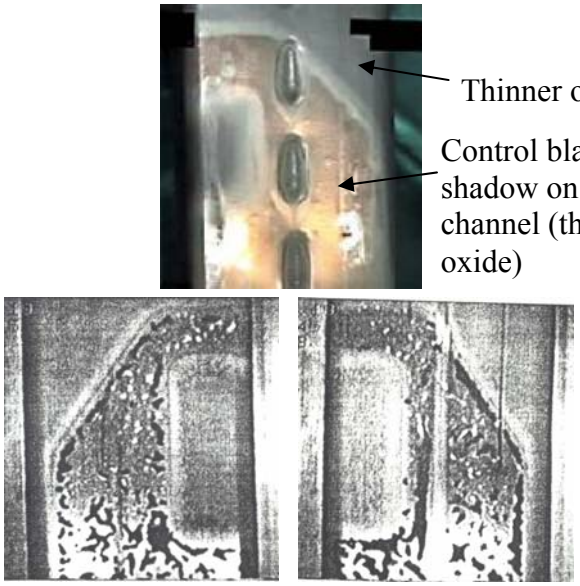

Figure 1. Typical shadow corrosion formed on the fuel channel next to control blade

While the shadow corrosion mechanism is not completely understood, it is known that a shadow corrosion requires two closely spaced dissimilar metals in an aqueous environment and radiation to form. There have been a few in-reactor loop tests designed to understand the shadow corrosion mechanism [1-4]. While some of these tests have greatly contributed to our understanding, the mechanism is still not understood clearly. The main proposed shadow corrosion mechanism is the galvanic type corrosion since there is a significant electrochemical potential difference between Zircaloy and dissimilar metals (inconel, stainless steel etc.) [3]. The galvanic corrosion hypothesis has many difficulties; for example, the role of irradiation in the galvanic corrosion process is not known. This hypothesis requires a direct contact or some ways to maintain the electrical conductivity between two dissimilar metals to accelerate the corrosion rate on fuel channel but it does not require the existence of irradiation.

The water radiolysis by β-radiation was proposed as an explanation for the shadow corrosion [5]. It was claimed that the beta radiation from neutron activation of Manganese, which is an alloying element in inconel and stainless steel, is responsible for the shadow corrosion on fuel channels. However, the amount of β-radiation from Manganese or any other elements in the BWR core have not been reported.

The objective of this analysis is to investigate radiation fields across the fuel channel, water gap, and control blade in a control cell of an operating BWR core with and without control blade

insertion and to shed a light on understanding of the radiation effect on the fuel channel shadow corrosion problem in BWR environment. Radiation fields across the fuel channel, water gap, and control blade are computed using MCNP5 to find the differences between the cases when the control blade is inserted and is not inserted.

2. COMPUTATION FOR RADIATION FIELDS

The MCNP5 is a widely used, general-purpose, continuous-energy, generalized-geometry, coupled neutron-photon-electron Monte Carlo transport computer program [6]. The neutron energy range is from 10^{-5} eV to 20 MeV, and the photon and electron energy range is from 1 keV to 1000 MeV in the MCNP. The bremsstrahlung radiation from rapidly moving electrons, and the low energy electrons and photons below 1 keV are not tracked in the MCNP.

2.1. Geometry of a Typical BWR Control Cell

A typical BWR control cell, which is composed of a control rod and four adjacent fuel bundles, is used in MCNP modeling. The modeled BWR control cell is shown in Figure 2. A typical 10x10 BWR fuel bundle consists of 92 fuel rods, two large central water rods and a channel. In this model, 4.26 wt.% lattice average uranium enrichment and 14 gadolinia fuel rods with 5 wt. % Gd enrichment were used.

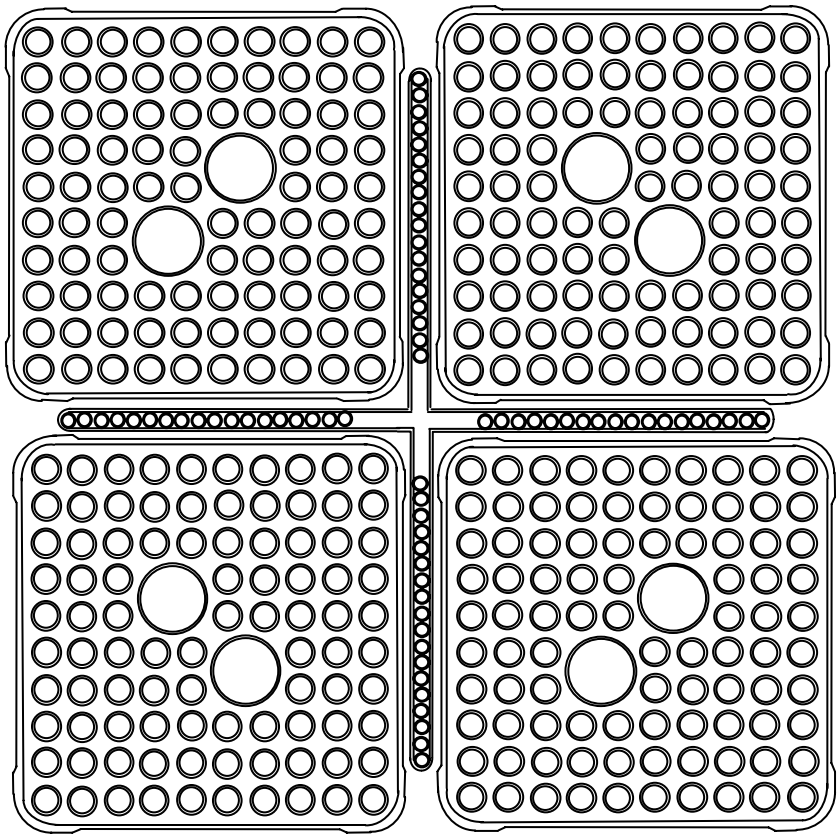

Figure 2. Geometry and cell structure of the BWR control cell used in the 2D modeling

2.2. Computational Model

The MCNP5 is used for computing radiation fields (neutron-gamma-electron) across the fuel channel, water gap, and the control blade with (controlled) and without (uncontrolled) the existence of control blades in the control cell. A control cell is simulated by applying the reflecting boundary condition on the four outer surfaces of an uncontrolled or controlled fuel bundle.

The MCNP lattice geometry input is composed of various cells and cell boundaries defined to represent the actual lattice configuration and tally regions. The MCNP lattice material composition input is composed of the atom concentrations of various nuclides and the associated cross section library data specification for all fuel types. The initial location and characteristics of neutron source is specified.

The ENDF/B-VI U235 and U238 cross section libraries at 527^{o}C in the MCNP cross section data set are used for the fuel in MCNP computation. The KCODE mode is run for each MCNP neutron-photon-electron coupled computation in an artificial steady state. The precision of the statistical MCNP computations depends on the number of neutron histories and a standard deviation is inversely proportional to the square root of number of tracked neutrons. Each MCNP run for this study carried out 420 batches computation with 10000 neutrons in each batch, which is considered to have 4.2 million neutron histories. The first 20 batch computational results are thrown out, since the neutron source distribution may not track the actual neutron source distribution well enough in initial batch runs.

The average fluxes of neutron, gamma, and electrons are tallied in a series of very thin nodes (20 μm x 1.2954 cm) next to the outer fifth fuel rod at channel surface (CS), water adjacent to channel (AC), water adjacent to blade (AB), and blade surface (BS) during the MCNP computations. The fluxes of the uncontrolled lattice are normalized to a power density of 54 kW/liter. On the other hand, the fluxes of the controlled lattice are normalized to a lower power density that is the product of 54 kW/liter and the ratio of the fission energy deposition in the controlled lattice over the fission energy deposition in the uncontrolled lattice.

2.3. Results and Discussion

The KCODE mode was run for each MCNP neutron-photon-electron coupled case by dividing the neutron fission source with an effective neutron multiplication factor, k_{eff}, such that the system behaves like an artificial steady state. The neutron multiplication factors and associated standard deviations (σ) of the two cases with 4.2 million neutron history are listed in Table 1.

Table 1. Neutron multiplication factors, k_{eff}, of two cases

Case	$k_{eff} \pm \sigma$
Uncontrolled	1.06061 ± 0.00032
Controlled	0.83712 ± 0.00034

The relative fission density distributions of the two cases are listed in Tables 2 and 3 and should be symmetric with respect to the diagonal line across the control rod central location. The slight

asymmetry of the relative fission density distributions with respect to the diagonal line is due to statistical nature of the MCNP computations.

Table 2. Relative fission density distribution of the uncontrolled case

1.246	1.279	1.302	1.327	1.306	1.297	1.297	1.317	1.243	1.213
1.285	1.154	0.362	1.029	1.071	1.062	0.965	0.352	1.076	1.238
1.302	0.361	0.830	0.949	1.003	1.024	0.341	0.764	0.350	1.291
1.330	1.036	0.948	0.837	1.119	0.000	0.000	0.336	0.920	1.250
1.313	1.078	1.013	1.122	1.247	0.000	0.000	0.959	0.955	1.270
1.301	1.060	1.035	0.000	0.000	1.216	1.063	0.883	0.341	1.234
1.294	0.958	0.343	0.000	0.000	1.062	0.778	0.858	0.917	1.293
1.329	0.352	0.767	0.336	0.958	0.890	0.859	0.771	0.350	1.280
1.256	1.081	0.350	0.923	0.946	0.341	0.907	0.351	1.101	1.278
1.224	1.241	1.298	1.248	1.271	1.239	1.290	1.280	1.275	1.201

Table 3. Relative fission density distribution of the controlled case

0.438	0.506	0.578	0.657	0.694	0.734	0.785	0.914	1.061	1.223
0.506	0.594	0.326	0.742	0.811	0.842	0.790	0.386	1.082	1.335
0.583	0.330	0.702	0.850	0.943	1.020	0.397	0.867	0.431	1.520
0.663	0.749	0.853	0.835	1.183	0.000	0.000	0.428	1.142	1.548
0.703	0.807	0.954	1.189	1.409	0.000	0.000	1.207	1.218	1.648
0.739	0.837	1.021	0.000	0.000	1.506	1.328	1.148	0.463	1.655
0.785	0.796	0.400	0.000	0.000	1.335	1.011	1.142	1.224	1.755
0.908	0.390	0.863	0.428	1.214	1.145	1.148	1.041	0.486	1.758
1.071	1.082	0.432	1.143	1.222	0.463	1.227	0.486	1.521	1.777
1.226	1.343	1.512	1.551	1.639	1.642	1.752	1.752	1.770	1.679

The fluxes of neutron, photon, and electron at Channel Surface (CS), water Adjacent to Channel (AC), water adjacent to blade (AB) next to the outer fifth fuel rod for both uncontrolled and controlled cases and at blade surface (BS) for controlled case are compared in Figure 3 at various radiation kinetic energies.

The neutron fluxes are practically the same above 100 eV due to long neutron mean free path and only show small differences below 100 eV between fuel channel, water adjacent to channel, water adjacent to control blade and at the control blade surface in the controlled case. Although the similar trend for the neutron spectrum is observed for uncontrolled case, the flux in uncontrolled case is higher than that in controlled case (especially in the thermal neutron part). The statistics of the neutron fluxes are quite good (lower than 1.5%) in all cases.

The photon fluxes are practically the same above 100 keV between fuel channel, water adjacent to channel, water adjacent to control blade and also at the control blade surface in the controlled case due to long gamma mean free path and only show small differences below 100 keV.

However, since the statistics of the low energy photon fluxes are quite poor (3%-95%) in the first three energy bins (1.5 keV - 7.5 keV), the differences on the calculated photon fluxes are not meaningful at 1.5 keV and lower energies. The photon fluxes calculated for controlled and uncontrolled cases are quite similar for all calculated points.

The electron fluxes show some differences, especially below 100 keV, between fuel channel, water adjacent to water adjacent to control blade and control blade surface primarily due to three factors: 1) short range of electrons, 2) dependence of Compton- and photon-electron productions on different atomic number Z among fuel channel, water and control blade, and 3) dominance of photoelectron production (approximately proportional to Z^4/E^3) from low energy photons in high Z material. The statistics on calculated electron fluxes are less than 10% except at high energy, which shows poor statistics at 7.5 MeV energy bin.

The low-energy electron fluxes (electron/cm^2-sec) at the channel surface (CS), water adjacent to channel (AC), blade surface (BS), and flux ratio between the channel surface and adjacent channel water (CS/AC) and between the channel surface and blade surface (CS/BS) next to the outer fifth fuel rod at different energies from 1.5 keV to 250 keV are compared in Table 4.

Table 4. Low-energy electron fluxes (electron/cm^2-sec) at channel surface (CS), adjacent channel water (AC), blade surface (BS), and flux differences between channel surface and adjacent channel water (CS-AC) and between channel surface and blade surface (CS-BS)

Energy	1.5 keV	3.5 keV	7.5 keV	30 keV	75 keV	250 keV
CS-U	1.74E+12	9.77E+11	7.12E+11	5.19E+11	5.20E+11	4.06E+11
AC-U	6.19E+11	4.60E+11	3.91E+11	3.90E+11	4.47E+11	3.91E+11
CS-C	1.12E+12	6.28E+11	4.60E+11	3.52E+11	3.66E+11	2.48E+11
AC-C	3.59E+11	2.57E+11	2.05E+11	2.44E+11	2.77E+11	2.19E+11
BS-C	8.37E+11	4.76E+11	3.39E+11	2.68E+11	2.77E+11	2.38E+11
(CS/AC)-U	2.8	2.1	1.8	1.3	1.2	1.0
(CS/AC)-C	3.1	2.4	2.2	1.4	1.3	1.1
(CS/BS)-C	1.3	1.3	1.4	1.3	1.3	1.0

Two phenomena can be observed from comparison of the MCNP electron flux results in Figure 3 and Table 4:

1) The ratio of low-energy electron fluxes between the channel surface and the water adjacent to channel become larger as the electron energy decreases for both the uncontrolled and controlled cases. This trend should continue for very low energy electrons with energy much less than 1 keV toward several eV, since the photoelectron production is approximately proportional to Z^4/E^3. However, there is lack of cross-section libraries for photons and electrons with energy lower than 1 keV in the MCNP.

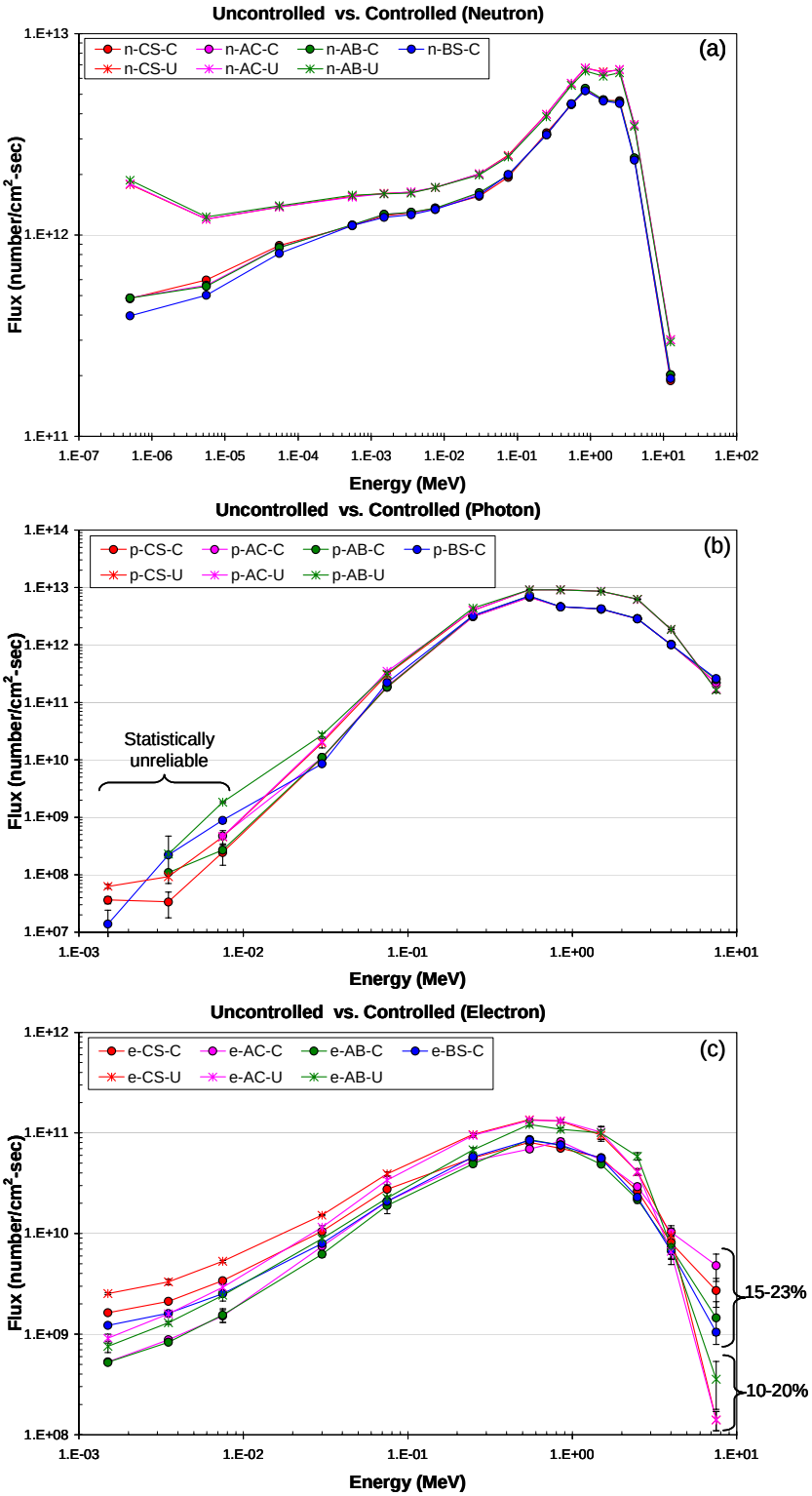

Figure 3. Comparison between (a) neutron fluxes, (b) photon fluxes, (c) electron fluxes for uncontrolled (no control blade inserted) and controlled (control blade inserted) cases

2) The ratio of low energy electron fluxes between the channel surface and the water adjacent to channel of the controlled case (CS/AC)-C are about the same as the corresponding low energy electron flux differences of the uncontrolled case (CS/AC)-U. This phenomenon should exist for very low energy electrons with energy much less than 1 keV toward several eV.

Based on comparison of the MCNP electron fluxes in Table 4, the low-energy electron fluxes at the channel surface (CS-C) are higher than the corresponding low-energy electron fluxes at the blade surface (BS) for electrons with kinetic energy below 250 keV. However, the ranges of low energy electrons are very short in the water, e.g., the range of 250 keV electron is 0.089 cm in the hot water between the fuel channel and the control blade in an operating BWR.

Under normal operating conditions, the modeling results show that there is no direct electron current from the Zr fuel channel surface to the stainless steel control blade surface through the water gap between these components due to larger distance than 0.089 cm. The net electron flow from the fuel channel surface to the control blade surface is possible only when the distance between the fuel channel and the control blade is less than 0.089 cm. It will happen only when a severe channel bow or a similar event occurs. If a net electron flow from the fuel channel surface to the control blade surface occurs, the corrosion rate of the fuel channel surface next to the control blade surface may be accelerated due to galvanic corrosion.

3. CONCLUSION

All forms of ionizing radiation interaction eventually result in a distribution of low energy electrons. The MCNP5 is used for computing radiation fields in the neighborhood of fuel channel of a typical 10x10 BWR fuel lattice with and without control blade insertion. The MCNP computational results indicate that 1) the neutron fluxes are practically the same above 100 eV and only show small differences below 100 eV between fuel channel and control blade in the controlled case, 2) the photon fluxes are practically the same above 100 keV and only show small differences below 100 keV between fuel channel and control blade, and 3) the electron fluxes show some differences, especially below 100 keV, among fuel channel, water gap and control blade. Practically no flux difference for neutrons above 100 eV and for photon above 100 keV in the neighborhood of fuel channel is due to long neutron and gamma mean free paths. The low energy electron flux differences are primarily due to three factors: 1) short range of electrons, 2) dependence of Compton- and photon-electron productions on different atomic number Z among channel, water and control blade, and 3) dominance of photoelectron production (approximately proportional to Z^4/E^3) from low energy photons in high Z material.

A net electron flow from the channel to the blade is possible only if a severe channel bow occurs such that the distance between the channel and the blade is less than 0.089 cm. This may lead to electron conduction between the fuel channel and the control blade. Therefore, it may enhance the channel shadow corrosion due to galvanic coupling. However, the MCNP modeling results show that it is not possible to have direct electron conduction between the fuel channel and control blade due to irradiation under normal operating conditions.

Even though some differences between photon and electron fluxes at the fuel channel surface, water, and the control blade surface are observed at low energy portion of the spectra, there are

many uncertainties in those regions. It is not known how complete the photon and electron cross-section libraries are in low energies in addition to lack of bremsstrahlung contribution. Moreover, we are limited by lack of the cross-section libraries lower than 1 keV for photon and electron flux calculations. Therefore, the effect of low energy electron and photon on shadow corrosion is not clear.

ACKNOWLEDGMENTS

The authors would like to acknowledge useful discussions with Dr. Boching Cheng of EPRI and a research funding from EPRI for this study.

REFERENCES

1. B. Andersson, M. Limback, G. Wikmark, E. Hauso, T. Johnsen, R. G. Ballinger and A.-C. Nystrand, "Test Reactor Studies of the Shadow Corrosion Phenomenon", *ASTM International*, pp. 583-615 (2002).
2. A. Chatelain, B. Andersson, R. G. Ballinger, and G. Wikmark, "Enhanced Corrosion of Zirconium-Base Alloys in Proximity to Other Metals: The Shadow Effect", *ANS International Topical Meeting on Light Water Reactor Fuel Performance*, Park City, Utah, April 10-13 (2000).
3. G. Lysell, A.-C. Nystrand, and M. Ullberg, "On the Shadow Corrosion Mechanism for Zirconium Alloys", *ENS Top Fuel Conference* (2001).
4. S. Shimada, K. Asahi, Y. Nonaka, M. Sasaki, T. Kogai, H. Hayashi, M. Kitamura, M. Sakamoto and M. Yamawaki, "Evaluation of Zircaloy-2 Cladding Corrosion Characteristics by Simulated BWR Corrosion Loop Test", *ASTM STP* 1354, pp. 735-755 (2000).
5. J.-S. F. Chen and R. B. Adamson, "Observation of Shadow Phenomena on Zirconium Alloys", *Proc. ANS 1994 Int'l Top. Meeting Light Water Reactor Fuel Performance,* West Palm Beach, FL, April 17-21 (1994).
6. LA-UR-03-1987, "MCNP_ A General Monte Carlo N-Particle Transport Code - Version 5", October (2005).